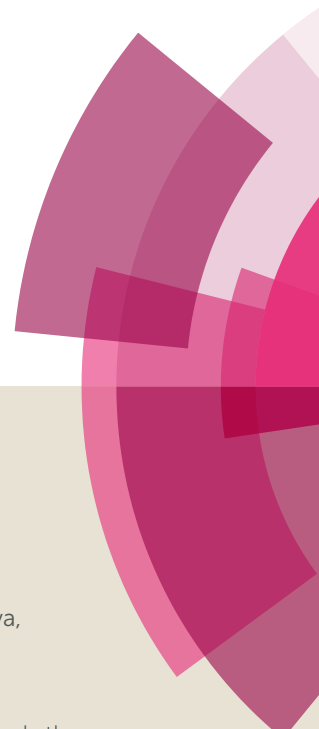


# NJC

Accepted Manuscript



This article can be cited before page numbers have been issued, to do this please use: E. Konstantinova, A. Minnekhanov, A. Beltiukov, V. Ivanov, A. J. Sutherland and O. Boytsova, *New J. Chem.*, 2018, DOI: 10.1039/C8NJ03196G.



This is an Accepted Manuscript, which has been through the Royal Society of Chemistry peer review process and has been accepted for publication.

Accepted Manuscripts are published online shortly after acceptance, before technical editing, formatting and proof reading. Using this free service, authors can make their results available to the community, in citable form, before we publish the edited article. We will replace this Accepted Manuscript with the edited and formatted Advance Article as soon as it is available.

You can find more information about Accepted Manuscripts in the [author guidelines](#).

Please note that technical editing may introduce minor changes to the text and/or graphics, which may alter content. The journal's standard [Terms & Conditions](#) and the ethical guidelines, outlined in our [author and reviewer resource centre](#), still apply. In no event shall the Royal Society of Chemistry be held responsible for any errors or omissions in this Accepted Manuscript or any consequences arising from the use of any information it contains.

## Unveiling point defects in titania mesocrystals: a combined EPR and XPS study

Elizaveta Konstantinova<sup>1,2,3\*</sup>, Anton Minnekhanov<sup>2</sup>, Artemii Bulyukov<sup>4</sup>, Vladimir Ivanov<sup>5,6</sup>, Andrew J. Sutherland<sup>7</sup> and Olga Boytsova<sup>5,6\*</sup>

<sup>1</sup>Department of Physics, Lomonosov Moscow State University, Leninskie Gory 1-2, 119991 Moscow, Russia

<sup>2</sup>National Research Center Kurchatov Institute, Kurchatov Square 1, 123182 Moscow, Russia

<sup>3</sup>Department of Nano-, Bio-, Information Technology and Cognitive Science, 141701 Dolgoprudny, Moscow Region, Russia

<sup>4</sup>Udmurt Federal Research Center of the Ural Branch of the Russian Academy of Sciences, 426000 Izhevsk, Russia

<sup>5</sup>Kurnakov Institute of General and Inorganic Chemistry Russian Academy of Sciences, Leninskii Ave. 31, 119991 Moscow, Russia

<sup>6</sup>Department of Materials Science, Lomonosov Moscow State University, Leninskie Gory 1-3, 119991 Moscow, Russia

<sup>7</sup>Aston Institute of Materials Research, Aston University, Aston Triangle, Birmingham, B4 7ET, UK.

### Author Information

Corresponding authors:

\* E-mails: Olga Boytsova (boytsova@gmail.com) and Elizaveta Konstantinova (liza35@mail.ru)

### Abstract

Titania mesocrystals, prepared using a polyethylene template, were studied by a combination of electron microscopy, XPS and EPR techniques. The electronic structure and local environment of point defects in the TiO<sub>2</sub> mesocrystals were deduced from experimental and simulated EPR data. The Ti<sup>3+</sup>/F centers and oxygen defects were shown to be the most photosensitive. The presence of carbon radicals was also demonstrated. Since the point defects govern TiO<sub>2</sub> photosensitivity and photocatalytic activity in the

visible spectral range, the data obtained provide new insights into photocatalytic reactions engineering using titania mesocrystals.

## Introduction

Engineering of self-assembled hybrid mesocrystals is one of the leading trends in synthetic materials. This unique type of material has a tremendous potential to revolutionize materials/devices based on inorganic components. Seeking to benefit from improved functional characteristics, many research groups have fabricated mesocrystals of different sizes, shapes and microarchitectures demonstrating enhanced effects in the properties of the resultant materials.<sup>1-8</sup> Interestingly, most studies so far have revealed that the characteristics of the self-assembled materials depend strongly on the synthetic procedures used in their generation.<sup>3</sup> The origin of specific functional properties (optical response, photocatalytic activity, mechanical hardness, elasticity, etc.) in these entities has been attributed to the fine interplay of crystal structure and surface state.<sup>2</sup>

Titania mesocrystals have only recently been described and are best viewed as an entirely new class of materials.<sup>7,9,10</sup> Microstructural features of TiO<sub>2</sub> mesocrystals have been investigated thoroughly by several research groups.<sup>11-13</sup> Obviously, to provide a complete understanding, it is necessary to supplement these data with the crystallographic information on titanium and oxygen coordination environments in the TiO<sub>2</sub> mesocrystals that would help to explain correctly the physical and chemical properties of these materials. Here, we provide a first report on the crystalline and defect structure of pure anatase TiO<sub>2</sub> mesocrystals prepared using poly(ethylene glycol)-6000 g/mol (PEG-6000). A complex analysis of mesocrystal formation conditions was performed to understand how they affected the structure and determined electronic structure and local environments of the mesocrystals. TiO<sub>2</sub> mesocrystals are seen as promising candidates for the generation of new photocatalytic devices due to the simplicity of their synthesis and high catalytic activity in degrading toxic compounds under illumination in the visible spectral range. Since paramagnetic defects (oxygen-related radicals) are responsible for the photodegradation of compounds<sup>14-16</sup>, electron paramagnetic resonance (EPR) technique combined with electron microscopy and X-ray photoelectron spectroscopy (XPS) were chosen as a primary source of information on the

structure of TiO<sub>2</sub> mesocrystals. This analytical strategy gave us the opportunity to better evaluate possible practical applications of the mesocrystals.

## Experimental

Our approach to the synthesis of Ti-based mesostructures using a poly(ethylene glycol) 6000 (PEG-6000) templating agent includes several stages. At first, (NH<sub>4</sub>)<sub>2</sub>TiF<sub>6</sub> (Sigma-Aldrich UK) 0.1 mol L<sup>-1</sup>, PEG-6000 (Alfa Chemicals Ltd.) and gelation agent H<sub>3</sub>BO<sub>3</sub> (Alfa Chemicals Ltd.) 0.2 mol L<sup>-1</sup> were dissolved in distilled water (30 mL) under continuous stirring. Upon complete dissolution of the reagents, the resultant gel was kept at 35 °C for 20 hours. This process led to the formation of a precipitate which was isolated by centrifugation/decantation and subsequently washed with water (3 x 20 mL) and acetone (3 x 20 mL). It is to be noted that higher concentrations of PEG-6000 template led to mesocrystal agglomeration while lower concentrations resulted in centralized defects.<sup>11</sup> Therefore, precise control over PEG-6000 concentration is crucial for fabrication of non-agglomerated and defect-free NH<sub>4</sub>TiOF<sub>3</sub> mesocrystals. In our previous study<sup>11</sup>, it was established that for the synthesis of mesocrystals with the highest photocatalytic activities, the optimal molar ratios of the reagents should be as follows: PEG-6000:(NH<sub>4</sub>)<sub>2</sub>TiF<sub>6</sub>:H<sub>3</sub>BO<sub>3</sub> = 1:2:4.<sup>11</sup> The resultant NH<sub>4</sub>TiOF<sub>3</sub> mesocrystals were heated in air at 450 °C for 2, 4 or 8 hours. Gaseous HF evolved during this thermally-induced, multi-step transformation of NH<sub>4</sub>TiOF<sub>3</sub> mesocrystals into TiO<sub>2</sub> mesocrystals.

X-ray photoelectron spectroscopy (XPS) measurements were performed using an Axis Ultra DLD (Kratos, UK) spectrometer equipped with a monochromatic Al K $\alpha$  X-ray source. The spectra were fitted by the Gaussian–Lorentzian convolution functions with simultaneous optimization of the background parameters.

Scanning electron microscopy (SEM) studies were performed on a Carl Zeiss NVision 40 high resolution scanning electron microscope.

Low temperature nitrogen adsorption measurements were conducted using an ATX-6 analyzer (Katakon, Russia). Before the measurements, samples (30–60 mg weight) were degassed at 200 °C for 30 min under a dry helium flow. Determination of the surface area was carried out by using the 5-point Brunauer, Emmett and Teller (BET) method at the relative pressure range of  $P/P_0 = 0.05 - 0.25$ .

Electron paramagnetic resonance (EPR) spectra were recorded using a Bruker ELEXSYS E500 EPR spectrometer with a working frequency of 9.5 GHz; X-band, sensitivity of about  $5 \times 10^{10}$  spin/G; modulation frequency 100 kHz. A  $\text{CuCl}_2 \cdot 2\text{H}_2\text{O}$  standard with a known number of spins was used to calculate the concentration of defects in the samples. A standard procedure was used to determine the defect concentration with reference to a standard sample.<sup>17</sup> The samples were irradiated in the optical cavity of the EPR spectrometer with a 50 W high-pressure mercury lamp (the spectral range is 245–900 nm) and a halogen lamp (the spectral range is 400–800 nm). The measurements were performed in the temperature range 10–300 K using a Bruker ER4112HV temperature control system. Computer simulation of the EPR signal was carried out using an EasySpin module of the MATLAB software package.<sup>18</sup> This procedure is necessary to obtain the most accurate values of the EPR spectral parameters (g,  $\Delta H$  values, etc.).

## Results and Discussion

In the present paper, a series of samples was investigated: initial  $\text{NH}_4\text{TiOF}_3$  mesocrystals and those heat-treated at 450 °C for 2, 4 and 8 hours (samples denoted as  $\text{TiO}_2$ -2T,  $\text{TiO}_2$ -4T and  $\text{TiO}_2$ -8T, respectively). The  $\text{NH}_4\text{TiOF}_3$  mesocrystals were generated from  $(\text{NH}_4)_2\text{TiF}_6$  and  $\text{H}_3\text{BO}_3$  in the presence of a PEG-6000 templating agent using methodology developed previously.<sup>11</sup>

Figure 1(a) shows the typical smooth form of a pristine  $\text{NH}_4\text{TiOF}_3$  mesocrystal. The morphology of the samples changed gradually upon annealing the pristine  $\text{NH}_4\text{TiOF}_3$  sample at 450 °C (Fig. 1, b-d). Smooth surfaces of the  $\text{NH}_4\text{TiOF}_3$  mesocrystals became rougher and considerably more porous. With an increase in the annealing time of the samples, the size of the  $\text{TiO}_2$  mesocrystals decreased. This can be explained by a loss of by-products from the thermally-mediated transformation of  $\text{NH}_4\text{TiOF}_3$  into  $\text{TiO}_2$  (e.g. HF) together with water and by-products from PEG-6000 decomposition (see XRD and atomic concentration of components of MCs at ESI S2 and S3 ).<sup>11</sup>

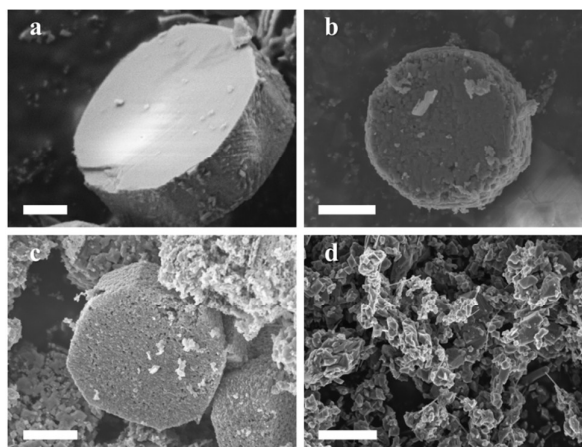


Figure 1. SEM images of Ti-based mesostructures: initial  $\text{NH}_4\text{TiOF}_3$  mesocrystals (a);  $\text{TiO}_2$ -2T (b),  $\text{TiO}_2$ -4T (c) and  $\text{TiO}_2$ -8T (d) samples. Scale bar is 1 (a, b, c,) and 2 (d) micron.

According to the BET measurements ( $\text{N}_2$  isotherm for  $\text{TiO}_2$  MCs presented at ESI, S4), the surface area of the samples at first increased with the annealing time and then it decreased (from  $1 \text{ m}^2/\text{g}$  for  $\text{NH}_4\text{TiOF}_3$ , up to  $20 \text{ m}^2/\text{g}$  for  $\text{TiO}_2$ -2T and  $\text{TiO}_2$ -4T and then down to  $7 \text{ m}^2/\text{g}$  for  $\text{TiO}_2$ -8T). These observations are consistent with the decomposition/loss processes, referred to above, giving a more porous open structure followed by loss of structural integrity upon prolonged heating resulting in a more condensed, collapsed nanocrystalline material with a concomitantly lower surface area. The SEM images in Figure 1 also support these findings.

Elemental composition of the samples under investigation was studied by XPS. Obtained results are shown in Figure 2 and Figure 3.

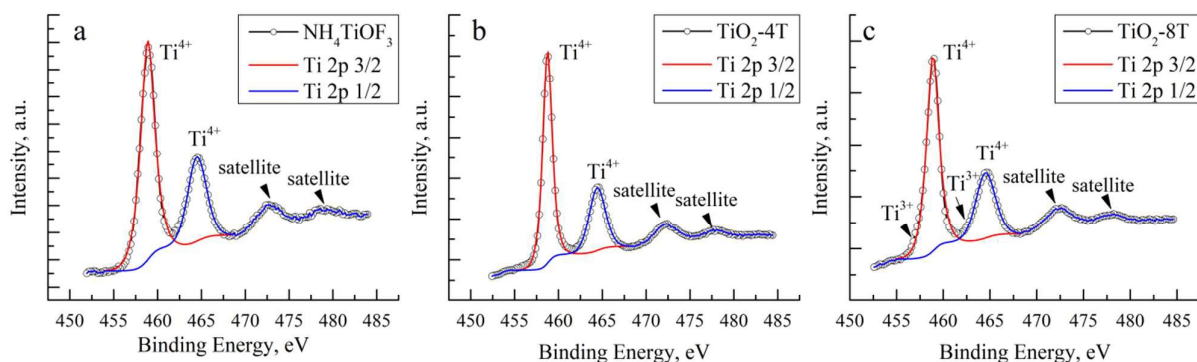


Figure 2. XPS spectra of the Ti 2p region of initial  $\text{NH}_4\text{TiOF}_3$  mesocrystals (a) and  $\text{TiO}_2$ -4T (b) and  $\text{TiO}_2$ -8T (c) samples.

XPS spectra in the Ti 2p binding energy range could be represented by contributions of two states: Ti 2p 3/2 and Ti 2p 1/2 (Figure 2). The Ti 2p peaks were symmetric and of high intensity, indicating that the samples contained only Ti<sup>4+</sup> surface species. After 8 hours of annealing, according to SEM images of the samples (Figure 1, d), almost complete destruction of the mesocrystals and formation of nanocrystal ensembles occurred, which was expected to be accompanied by an increase in the number of Ti<sup>3+</sup> surface centers. In the XPS spectra, due to the low concentration of Ti<sup>3+</sup>, it was not possible to deconvolute the corresponding lines from the bulk Ti<sup>3+</sup> centers (their positions are marked with arrows (Figure 2,c)).

Figure 3 shows XPS spectra corresponding to the O 1s binding energy range and is entirely consistent with previous studies so demonstrating the reproducibility of the synthetic process.<sup>11</sup> The main central line in all spectra refers to lattice oxygen. The relatively small right shoulder of the spectrum (532.2 eV) has previously been attributed to fluorine replacing oxygen in the titania lattice.<sup>11</sup> The intensity of this band decreases with increasing annealing time, which can be explained by a decrease in the fluorine content in the samples.<sup>11</sup> Similarly we have previously attributed the relatively minor left shoulder of the spectrum (529.9 eV) to the presence of carbonaceous admixtures from the PEG-6000 template, used during the synthesis. A decrease in the intensity of this line was also explained by the removal of PEG-6000 matrix residues during the annealing process.<sup>11</sup>

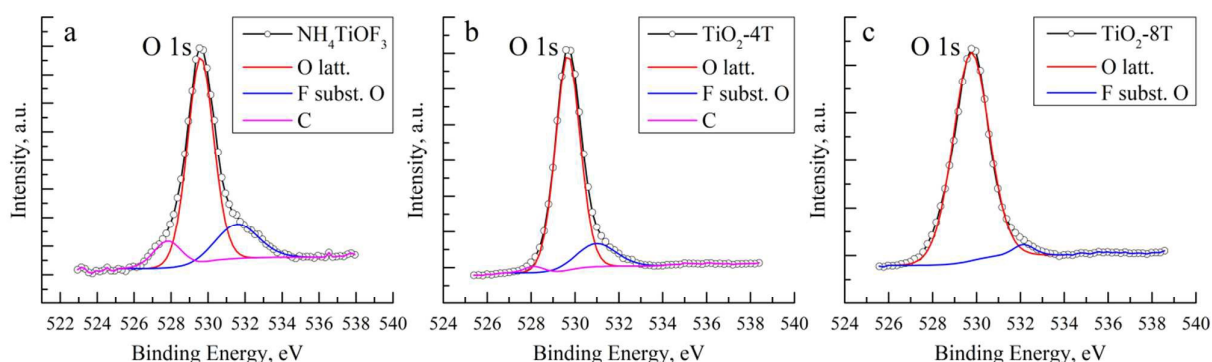


Figure 3. XPS spectra of the O 1s region of initial NH<sub>4</sub>TiOF<sub>3</sub> mesocrystals (a) and TiO<sub>2</sub>-4T (b) and TiO<sub>2</sub>-8T (c) samples.

Let us now discuss the features of the point defect formation in titania mesocrystals and their variations in the process of mesocrystal transformation into ensembles of nanocrystals during sample annealing. An EPR study of all samples at 300 K showed the absence of paramagnetic defects in these structures. The possible reason can be as follows: (i) the samples contained no paramagnetic defects; (ii) some of the defects were in a non-paramagnetic state, and, as a result, the concentration of defects was below the sensitivity limit of the EPR spectrometer; (iii) the relaxation times of defects were too short, which led to the large width of the lines in the EPR spectrum (due to the Heisenberg uncertainty principle) and, consequently, the impossibility of their detection. A simple way to change the charge state of defects was to illuminate the samples by a wide range of wavelengths to initiate both fundamental and impurity absorption of light. Trapping of photoexcited electrons and holes can lead to a change of the paramagnetic state of defects to a non-paramagnetic one and vice versa. This effect was reliably demonstrated in our previous papers.<sup>19-21</sup> The illumination (245–900 nm) of the samples did not lead to the appearance of any EPR signals. Yet, another reason existed for the absence of signals in the EPR spectrum. It is well known that the spin-lattice relaxation time can be controlled by changing the recording temperature of the EPR spectra.<sup>22,23</sup> A decrease in temperature leads to "freezing out" of phonon modes, the energy transfer from excited electron spins to phonons proceeds more slowly, and the width of the EPR signal line decreases. For TiO<sub>2</sub> mesocrystals, such a behaviour is quite typical: EPR signals were reliably recorded in the TiO<sub>2</sub> meso- and nanocrystals at low temperatures (Figure 4, 5). No paramagnetic defects were found in the initial NH<sub>4</sub>TiOF<sub>3</sub> mesocrystals (Figure 4, inset). This is supposedly due to a very low specific surface area (see above) and the presence of a high quantity of PEG-6000, which prevented the generation of point defects with unpaired electron spins. Indeed, the smaller the specific surface area, the lower the concentration of surface defects.<sup>23</sup> In turn, the presence of PEG promotes the formation of chemical bonds and a reduction in the number of unpaired electrons.

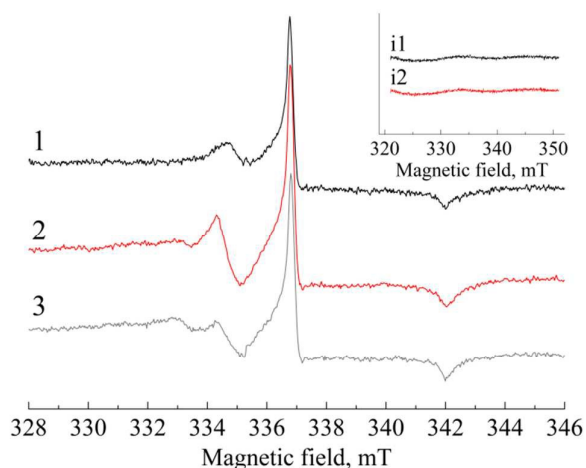


Figure 4. EPR spectra of TiO<sub>2</sub>-2T sample: (1) in the dark, (2) under illumination (5 min), (3) after illumination (10 min). T=20 K. Inset to Figure 4. EPR spectra of NH<sub>4</sub>TiOF<sub>3</sub> mesocrystals in the dark (1) and under illumination (2). T=20 K.

As follows from Figures 4 and 5, the EPR spectra of titania samples had a complex shape that was a result of the anisotropy of the EPR signals and the superposition of several EPR signals originating from various defect species. In addition, the shape and the intensity of the EPR lines underwent changes under illumination. Moreover, this effect was reversible (Figure 4), which is evidence of photoinduced processes of defect recharging. In turn, control experiments revealed that all TiO<sub>2</sub> samples were very photosensitive under both UV and VIS illumination, i.e. their EPR spectra underwent photoinduced changes. Taking into account possible practical application, the following experiments were conducted under visible light illumination (400-800 nm). To analyze these EPR spectra, computer simulation was used (EasySpin module of MATLAB software). The corresponding results are shown in Figure 5.

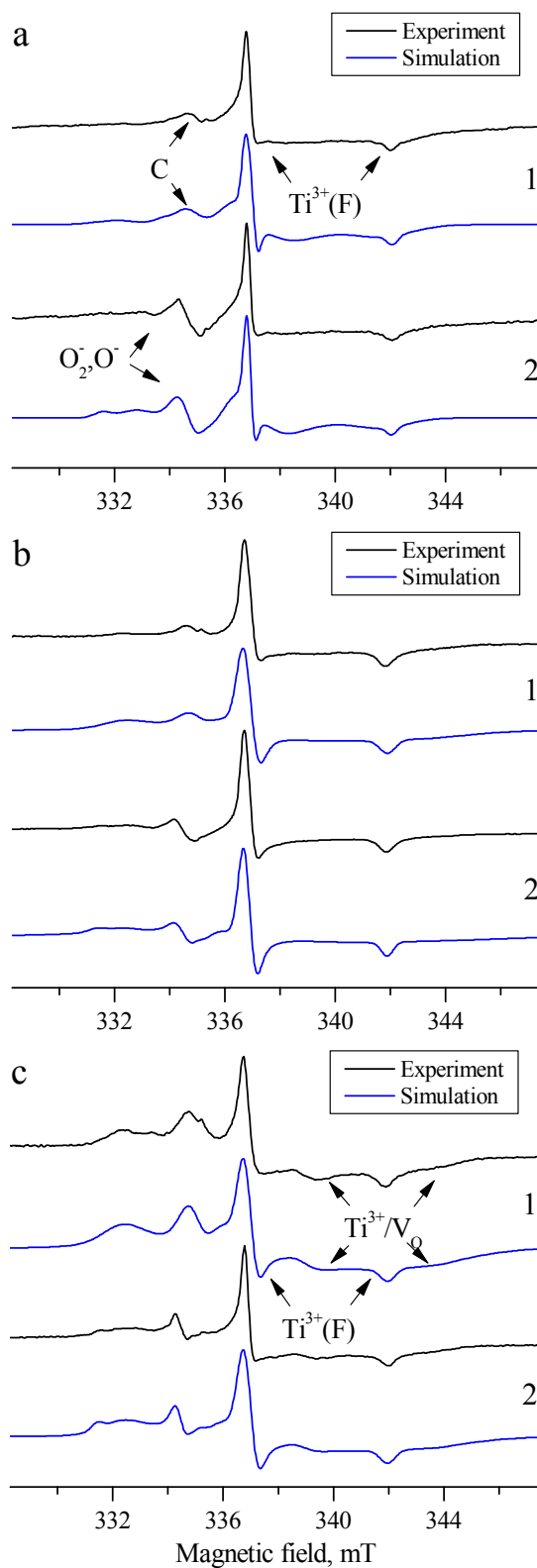


Figure 5. Normalized experimental and theoretical EPR spectra of TiO<sub>2</sub>-2T (a), TiO<sub>2</sub>-4T (b), TiO<sub>2</sub>-8T (c) in the dark (1) and under illumination (2). T = 20 K.

From computer simulations of EPR spectra the main parameters of the EPR signals – g-tensor and line width values were deduced:  $g_1 = 1.9896 \pm 0.0002$ ,  $g_2 = 1.9600 \pm 0.0002$ ,  $\Delta H_1 = 6$  G,  $\Delta H_2 = 6$  G (EPR signal of I type);  $g_1 = 2.0223 \pm 0.0002$ ,  $g_2 = 2.0094 \pm 0.0002$ ,  $g_3 = 2.0031 \pm 0.0002$ ,  $\Delta H_1 = 4.8$  G,  $\Delta H_2 = 3.8$  G,  $\Delta H_3 = 5.3$  G (EPR signal of II type);  $g_1 = 2.02012 \pm 0.0002$ ,  $g_2 = 2.0090 \pm 0.0002$ ,  $g_3 = 2.0020 \pm 0.0002$ ,  $\Delta H_1 = 7.4$  G,  $\Delta H_2 = 6.1$  G,  $\Delta H_3 = 8.1$  G (EPR signal of III type);  $g = 2.0040 \pm 0.0002$ ,  $\Delta H = 8.8$  G (EPR signal of IV type). Comparing obtained g-factor values with literature data, we concluded that the samples contained the following paramagnetic centers: type I corresponded to the  $Ti^{3+}$  spin center in  $Ti^{4+}-F-Ti^{3+}$  species<sup>24</sup>; type II corresponded to  $O_2^-$  radicals<sup>25-30</sup>; type III corresponded to  $O^-$  radicals<sup>25,31,32</sup>; type IV corresponded to  $C^\bullet$  radicals.<sup>33</sup> There is a little trace of  $Ti^{3+}$  spin center in  $Ti^{4+}-V_O-Ti^{3+}$  species<sup>25,34,35</sup> (here,  $V_O$  is oxygen vacancy) in the samples — EPR signal of type V with parameters:  $g_1 = 1.9784 \pm 0.0002$ ,  $g_2 = 1.9490 \pm 0.0002$ ,  $\Delta H_1 = 10$  G,  $\Delta H_2 = 10$  G. A contribution of  $Ti^{4+}-V_O-Ti^{3+}$  species is maximal for  $TiO_2-8T$  samples. It is notable that the most intensive EPR signal (type I) belongs to the  $Ti^{3+}/F$  defects, which were observed in all  $TiO_2-2T$ ,  $TiO_2-4T$ ,  $TiO_2-8T$  samples. The left shoulder of the  $Ti^{3+}/F$  EPR signal is due to  $C^\bullet$  radicals. The  $Ti^{3+}/V_O$  defects (very weak peaks on right shoulder of  $Ti^{3+}/F$  EPR signal) were detected in  $TiO_2-8T$  nanocrystals only, which was attributed to the fluorine loss during long-term sample annealing. Because of the very low number of  $Ti^{3+}/V_O$  centers we could not extract them from the XPS data (see above).

At 20 K the EPR signal from  $Ti^{3+}/F$  defects has a high intensity. Therefore it is very complicated to observe an appearance of EPR signals attributed to the oxygen radicals ( $O_2^-$ ,  $O^-$ ) under illumination. Because of this we have measured the EPR spectra of all of the samples at 120 K (Figure 6). We can see from Fig. 6 that the  $Ti^{3+}/F$  EPR signal intensity is comparable with one of the oxygen radicals. As Fig. 6 indicates, our samples are very photosensitive under illumination: this results in the appearance of EPR signals from oxygen radicals and simultaneously  $Ti^{3+}$  centers and the EPR signal intensity growing.

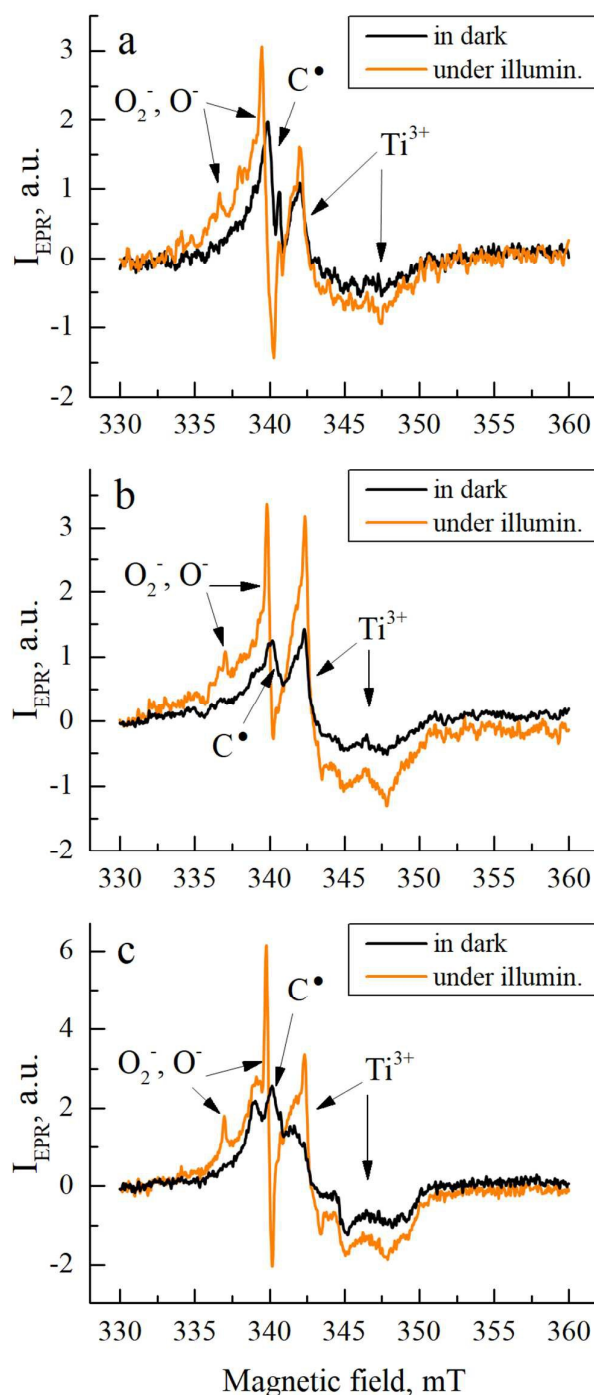


Figure 6. Experimental EPR spectra of  $\text{TiO}_2\text{-2T}$  (a),  $\text{TiO}_2\text{-4T}$  (b),  $\text{TiO}_2\text{-8T}$  (c) in the dark and under illumination.  $T = 120$  K.

The concentration of the  $\text{Ti}^{3+}/\text{F}$  defects increased under illumination (Figure 4). We assumed that the defects were partly in non-paramagnetic state ( $\text{Ti}^{4+}/\text{F}$ ). Under illumination, a large number of photoexcited electrons were formed, which were captured by the non-paramagnetic  $\text{Ti}^{4+}/\text{F}$  centers. The latter transformed to the paramagnetic  $\text{Ti}^{3+}/\text{F}$

state, and the growth of the EPR signal intensity was observed (Figure 4). Oxygen-related radicals ( $O_2^-$  and  $O^-$ ) were formed mainly under illumination (Figures 5 and 6) according to the following reactions:  $h\nu + TiO_2 \rightarrow e^- + h$ ,  $O_2 + e^- \rightarrow O_2^-$  and  $O^{2-} + h \rightarrow O^-$ , respectively.<sup>36</sup>

We have calculated the overall concentrations of all the defects in the samples under investigation (Table 1). It should be noted that the highest concentration of defects was detected in  $TiO_2$ -4T samples. These samples exhibited the best photocatalytic activity according to our previous data.<sup>11</sup> The main contribution to the EPR signal is given by  $Ti^{3+}/F$  and  $O_2^-$ ,  $O^-$  defects (see Figure 6). Therefore, comparing the results obtained in this paper with ones from our previous work<sup>11</sup>, we suppose, that the  $Ti^{3+}/F$  and oxygen radicals in  $TiO_2$  mesocrystals could play a key role in photocatalytic degradation of organic pollutants.

Table 1. Concentration of defects in the samples.

Sample	Concentration, $g^{-1}$	
	In the dark	Under illumination (20 min)
$TiO_2$ -2T	$(8.9 \pm 0.9) \cdot 10^{14}$	$(1.5 \pm 0.2) \cdot 10^{15}$
$TiO_2$ -4T	$(2.3 \pm 0.2) \cdot 10^{15}$	$(6.5 \pm 0.3) \cdot 10^{15}$
$TiO_2$ -8T	$(1.9 \pm 0.1) \cdot 10^{15}$	$(3.7 \pm 0.2) \cdot 10^{15}$

## Conclusions

Titania mesocrystals were synthesized by a previously established technique, based on thermal decomposition of PEG-6000 templated mesocrystals of  $NH_4TiOF_3$ . The key advantage of this method is that it uses simple chemical transformations to create smooth, regular and uniformly-sized  $NH_4TiOF_3$  mesocrystals and that this general mesostructure is retained in thermally-mediated conversion into  $TiO_2$  mesocrystals as long as heating times are not overly long. EPR-spectroscopy was shown to be an efficient tool for the identification and quantitative analysis of the defects in  $TiO_2$  mesocrystals.  $TiO_2$  mesocrystals were found to contain mainly  $Ti^{3+}$  defects having fluorine in the local environment which replaced the oxygen atoms in the titania lattice. Long-term annealing of  $TiO_2$  mesocrystals led to an increase of  $Ti^{3+}$ /oxygen vacancy defects. Besides,  $TiO_2$  mesocrystals were characterized by the presence of some quantity of carbon radicals. It

was established that under visible illumination, the density of  $\text{Ti}^{3+}/\text{F}$  centers was increased and oxygen-related radicals are generated. This result correlates well with our previous reported data on the photocatalytic activity of titania-based nanostructures.<sup>11</sup> Collectively, these are important experimental facts that will help inform techniques for the generation of  $\text{TiO}_2$  mesocrystals, for use in photocatalytic applications, with superior properties to those available currently.

### Conflicts of interest

There are no conflicts to declare.

**Electronic Supplementary Information (ESI) available:** [XRD and XPS data, Full isotherm of  $\text{N}_2$  adsorption].

### Acknowledgments

We acknowledge the support of the European Commission (Grant PolyCOMP no. 661317) and RF President Grant (MK-336.2017.3). EPR measurements were performed using the facilities of the Collective Use Center at the Moscow State University and in frame of the Program of development of M.V. Lomonosov Moscow State University.

### References

1. H. Cölfen and M. Antonietti, *Angew. Chem. Int. Ed.*, 2005, **44**, 5576.
2. E. V. Sturm and H. Cölfen, *Chem. Soc. Rev.*, 2016, **45**, 5821.
3. V. K. Ivanov, P. P. Fedorov, A. Y. Baranchikov and V. V. Osiko, *Russ. Chem. Rev.*, 2014, **83**, 1204.
4. L. Zhou and P. O'Brien, *Small*, 2008, **4**, 1566.
5. L. Zhou and P. O'Brien, *J. Phys. Chem. Lett.*, 2012, **3**, 620.
6. H. Cölfen and S. Mann, *Angew. Chem. Int. Ed.*, 2003, **42**, 2350.
7. L. D. Zhou, D. Smyth-Boyle and P. O'Brien, *J. Am. Chem. Soc.*, 2008, **130**, 1309.
8. R.-Q. Song and H. Cölfen, *Adv. Mater.*, 2010, **22**, 1301.
9. L. Zhou, D. S. Boyle and P. O'Brien, *Chem. Commun.*, 2007, **0**, 144.

10. L. Zhou and P. O'Brien, *Phys. Status Solidi A*, 2008, **10**, 2317.
11. O. V. Boytsova, A. A. Sadovnikov, K. E. Yorov, A. N. Beltiukov, A. E. Baranchikov, V. K. Ivanov, X. Zhong, D. J. Lewis, P. O'Brien and A. J. Sutherland, *CrystEngComm.*, 2017, **19**, 3281.
12. Y. Liu, Y. Zhang and J. Wang, *CrystEngComm*, 2013, **15**, 791.
13. M. Inoguchi, M. Afzaal, N. Tanakaa and P. O'Brien, *J. Mater. Chem.*, 2012, **22**, 25123.
14. Y. Kikuchi, K. Sunada, T. Iyoda, K. Hashimoto and A. Fujishima, *J. Photochem. Photobiol. A: Chem.*, 1997, **106**, 51.
15. A. Fujishima and X. Zhang, *C. R. Chimie*, 2006, **9**, 750.
16. D. Dvoranová, Z. Barbieriková and V. Brezová, *Molecules*, 2014, **19**, 17279.
17. P. W. Atkins and M. C. R. Symons, *The Structure of Inorganic Radicals*, Elsevier Amsterdam -New York, **1967**.
18. S. Stoll and A. Schweiger, *J. Magn. Reson.*, 2006, **178**, 42.
19. A. Tarasov, A. Minnekhanov, G. Trusov, E. Konstantinova, A. Zyubin, T. Zyubina, A. Sadovnikov, Yu. Dobrovolsky and E. Goodilin, *J. Phys. Chem. C*, 2015, **119**, 18663.
20. N. T. Le, E. A. Konstantinova, A. I. Kokorin, T. Kodom and N. Alonso-Vante, *Chemical Physics Letters*, 2015, **635**, 241.
21. A. Tarasov, G. Trusov, A. Minnekhanov, D. Gil, E. Konstantinova, E. Goodilin and Yu. Dobrovolsky, *J. Mater. Chem. A*, 2014, **2**, 3102.
22. C. P. Poole and F. Horacio, *Theory of Magnetic Resonance. 2nd Ed.*, Wiley, New York **1987**.
23. J. A. Weil and J. R. Bolton, *Electron Paramagnetic Resonance: Elementary theory and Practical application*, John Wiley and Sons, Inc., Hoboken, New Jersey **2007**.
24. M. Chiesa, M. C. Paganini, S. Livraghi and E. Giamello, *Phys. Chem. Chem. Phys.*, 2013, **15**, 9435.
25. A. I. Kokorin, in *Chemical physics of nanostructured semiconductors*, ed. A. I. Kokorin and D. W. Bahnemann, VSP, **2003**, Chapter 8 Electron Spin Resonance of Nanostructured Oxide Semiconductors, 264.
26. R. F. Howe and M. J. Grätzel, *J. Phys. Chem.*, 1987, **91**, 3906.
27. I. S. Pentegov and E. A. Konstantinova, *Phys. Status Solidi C*, 2011, **8**, 1954.

28. E. A. Konstantinova, V. Y. Gayvoronskiy, V. Y. Timoshenko and P. K. Kashkarov, *Semiconductors*, 2010, **44**, 1059.
29. E. V. Skorb, E. A. Ustinovich, A. I. Kulak, D. V. Sviridov, *J. Photochem. Photobiol. A*, 2008, **193**, 97.
30. M. Vanhaelst, P. Clauws, *Phys. Stat. Sol. (b)*, 1978, **87**, 719.
31. J. H. C. Van Hooff, *J. Catal.*, 1968, **11**, 277.
32. V. Brezová, Z. Barbierikova, M. Zikalova, D. Dvoranová and L. Kavan, *Catalysis Today*, 2014, **230**, 112.
33. E. A. Konstantinova, A. I. Kokorin, S. Sakthivel, H. Kisch and K. Lips, *CHIMIA*, 2007, **61**, 810.
34. P. C. Gravelle, F. Juillet, P. Mériaudeau and S. Teichner, *J. Faraday Discuss. Chem. Soc.*, 1971, **52**, 140.
35. K. M. Reddy, S. V. Manorama, A. R. Reddy, *Mater. Chem. Phys.*, 2003, **78**, 239–245.
36. J. Schneider, M. Matsuoka, M. Takeuchi, J. Zhang, Y. Horiuchi, M. Anpo, *Chem. Rev.*, 2014, **114**, 9919.